Evidence for Long-Range Glycosyl Transfer Reactions in the Gas Phase

Andreas H. Franz and Carlito B. Lebrilla
University of California, Davis, Davis, California, USA

A long-range glycosyl transfer reaction was observed in the collision-induced dissociation Fourier transform (CID FT) mass spectra of benzylamine-labeled and 9-aminofluorene-labeled lacto-*N*-fucopentaose I (LNFP I) and lacto-*N*-difucohexaose I (LNDFH I). The transfer reaction was observed for the protonated molecules but not for the sodiated molecules. The long-range glycosyl transfer reaction involved preferentially one of the two L-fucose units in labeled LNDFH I. CID experiments with labeled LNFP I and labeled LNFP II determined the fucose with the greatest propensity for migration. Further experiments were performed to determine the final destination of the migrating fucose. Molecular modeling supported the experiments and reaction mechanisms are proposed. (J Am Soc Mass Spectrom 2002, 13, 325–337) © 2002 American Society for Mass Spectrometry

Structural elucidation of oligosaccharides from natural sources is very important in view of the key roles that glycans play in cognitive and adhesive processes in biological systems. Oligosaccharides are essential in fertilization [1], cell growth [2–4], inflammation [5], and post-translational protein modification [6–8]. Whereas the insight into the physical process of carbohydrate recognition is in its infancy, considerable progress has been made towards the quantitation and structural elucidation of biologically active oligosaccharides. NMR [9] yields structural information about oligosaccharides. Frequently, however, an inherent problem is the limited amount of sample causing NMR experiments to become time-consuming or impossible. The sensitivity and accuracy of mass spectrometry has made this technique the best choice for analysis of oligosaccharides [10, 11]. Structural information can be derived from collision-induced dissociation (CID) [12–20] or from post-source decay (PSD) time-of-flight (TOF) experiments [21–26]. Fragmentation of glycosidic bonds provides information about the monosaccharide sequence and computer algorithms can extract sequence information from web-based catalogs of MS^n spectra [27]. However, the assignment of anomeric configuration [28–35] and linkage [18, 36–38] within the oligosaccharide structure is not a trivial task. Glycosidase digestion [13, 39–47] in conjunction with mass spectrometric analysis can be used to assign linkage and stereochemistry. In an alternative approach, CID-fragmentation patterns have been linked to structural motifs in the oligosaccharide (catalog library approach) [12].

We recently reported on the use of more nucleophilic benzylogous amines, such as benzylamine and 9-aminofluorene, for the labeling of oligosaccharides and the experimental results of FT-MS experiments with the labeled oligosaccharides [48]. Detection of 5 pmol of 9-amino fluorene-labeled oligosaccharide was achieved with a photo diode array during HPLC separation. The label combines low cost with good nucleophilicity and ease of introduction. The behavior of oligosaccharides derivatized with benzylogous amines such as benzylamine in CID experiments has not been reported, although data obtained from PSD matrix-assisted laser desorption/ionization (MALDI)-TOF experiments have been published [25, 49].

In this paper, we discuss a long-range glycosyl transfer that occurs during CID for benzylamine- and 9-AmFL-labeled oligosaccharides. The transfer of a fucose across three monosaccharide units was observed only in protonated molecules. To the best of our knowledge, long-range transfers during CID experiments have only been reported twice in the literature [50, 51]. Examples for short-range transfers (over one saccharide residue) have been reported for several linear and branched oligosaccharides [52–54]. Thomas-Oates and co-workers [52, 53] reported internal residue losses that were due to short-range transfers. Earlier, McNeil [54] had observed the phenomenon of internal residue loss from per-O-alkylated oligosaccharides, with no mechanistic explanation put forth. Interestingly, short-range transfers have also been reported for protonated peptides suggesting similar migration reactions [55].

Published online February 13, 2002

Address reprint requests to Dr. C. B. Lebrilla, Department of Chemistry, University of California, Davis, One Shields Avenue, Davis, CA 95616, USA. E-mail: cblebrilla@ucdavis.edu

1044-0305/02/$20.00
PII S1044-0305(02)00343-4

Received November 27, 2001
Revised December 26, 2001
Accepted December 26, 2001

Experimental

Unless stated otherwise, the chemicals used in the derivatization reaction were purchased from Sigma-Aldrich (St. Louis, MO) and used without further purification. Solvents were of HPLC grade. Oligosaccharides were purchased from Oxford Glycosystems (Rosedale, NY). Evaporation of small amounts of solvent was done on a Centrivap Concentrator (Labconco Corporation, Kansas City, MO) at 45 °C. Porous graphitized carbon (PGC) cartridges for desalting were purchased from Alltech Associates, Inc. (Deerfield, IL).

Mass spectra were recorded on an external source HiResMALDI (IonSpec Corporation, Irvine, CA) equipped with a 4.7 tesla magnet [12, 56–58] The HiResMALDI was equipped with an LSI 337 nm nitrogen laser. 2,5-Dihydroxy-benzoic acid was used as matrix (5 mg/100 μL in ethanol). A 0.01 M solution of NaCl in methanol was used as dopant. An NH_4-resin was used to remove alkali metals and produce the protonated species.

General Procedure for Labeling with 9-Aminofluorene

The oligosaccharide (200 nmol) was dissolved in nanopure water (50 μL) in a plastic microcentrifuge tube (2 mL). In another microcentrifuge tube 9-aminofluorene hydrochloride (2 mol equivalents) was dissolved in water (200 μL). This solution was treated with $NaHCO_3$ (1 mol equivalent with respect to the label) to give the free amine as white precipitate. After ten minutes at room temperature, the suspension was evaporated in vacuo and the remainder was dissolved in methanol (100 μL). To this solution $NaCNBH_3$ (3 mg, 0.05 mmol) was added followed by glacial acetic acid (5 μL). The resulting reagent solution was added immediately to the above solution of the oligosaccharide in water. The reaction mixture was heated to 80 °C for 2 h in a closed microcentrifuge tube. After 2 h the reaction mixture was cooled to room temperature and was evaporated in vacuo. The labeled oligosaccharide was dissolved in nanopure water (100 μL) and was desalted by a method adapted from the literature [59]. A PGC cartridge was washed with an aqueous solution with 80% (vol/vol) acetonitrile and 0.05% (vol/vol) trifluoroacetic acid (15 mL total) at a flow rate of about 3 mL/min. The solution of the labeled oligosaccharide was applied to the PGC cartridge. Subsequently the cartridge was washed with nanopure water (15 mL total) at a flow rate of about 1 mL/min followed by an aqueous solution with 60% (vol/vol) acetonitrile and 0.05% (vol/vol) trifluoroacetic acid (15 mL total). The UV-active fractions were collected and concentrated in vacuo for mass spectrometric analysis.

General Procedure for Labeling with Benzylamine

The oligosaccharide (200 nmol) was dissolved in nanopure water (50 μL). In a separate vial benzylamine (10 μL) was dissolved in methanol (100 μL). To this solution was added $NaCNBH_3$ (3 mg, 0.05 mmol) followed by glacial acetic acid (5 μL). The resulting reagent solution was added immediately to the above solution of the oligosaccharide in water. The reaction mixture was heated to 80 °C for 2 h. Workup was performed as described (vide supra).

Mass Spectrometric Analysis (MALDI-FTMS)

The solution of the labeled oligosaccharide (1 μL) was applied to the MALDI probe followed by sodium dopant (1 μL) or NH_4-resin and matrix solution (1 μL). The sample was dried under a stream of air and subjected to mass spectrometric analysis. For all CID experiments, the appropriate isolation pulses were programmed starting at 3 s after the initial ionization and followed by SORI excitation at 6 s (1 s, 5 V base to peak, +1000 Hz off-resonance). At a background pressure of 10^{-10} torr, argon gas was administered through a pulsed valve at 6 and at 6.5 s (peak pressure 5×10^{-5} torr). Final excitation for detection was performed 12 s after the initial laser pulse.

Molecular Modeling

The molecule was constructed and pre-minimized in the consistent valence force field (CVFF) implemented in the Insight II program as previously described [60]. Temperature annealing was done by heating the molecule to 600 K for 200 ps. Every 8 ps a sample snapshot was taken from the trajectory of the molecule and annealed to 0K. In this way, 25 structures were obtained. Structures that were within 3 kcal/mol of the lowest energy were kept and superimposed.

Results and Discussion

Lacto-*N*-difucohexaose I (LNDFH I) and lacto-*N*-difucohexaose II (LNDFH II) were derivatized with 9-AmFL to give Compounds **1** and **2** (Scheme **1**) and CID spectra were recorded (Figure 1). The sodium-doped sample of **1** produced the quasimolecular ion at *m/z* 1187. The CID of this ion gave rise to fragment ions consistent with the molecular structure (Figure 1a). The formal fragmentation nomenclature for the assignment of oligosaccharides has been published by Domon and Costello [61]. Fragment ions with *m/z* 1041 ($Y_{4\alpha}$ or $Y_{3\beta}$), 895 ($Y_{4\alpha}/Y_{3\beta}$), 879 ($Y_{3\alpha}$), 733 ($Y_{3\alpha}/Y_{3\beta}$), and 530 (Y_2) were observed. Additionally, loss of labeled residues from $[M + Na]^+$ gave rise to a different series of fragment ions consisting of ions at *m/z* 842 (B_4), 714 ($Y_{4\alpha}/C_4$), and 696 ($Y_{4\alpha}/B_4$ or $B_4/Y_{3\beta}$). The fragment ion at *m/z* 696 further gave rise to the loss of a fucose (*m/z* 550, $B_4/Y_{4\alpha}/Y_{3\beta}$), a galactose (*m/z* 534, $B_4/Y_{3\alpha}$), and both (*m/z* 388, $B_4/Y_{3\alpha}/Y_{3\beta}$). The

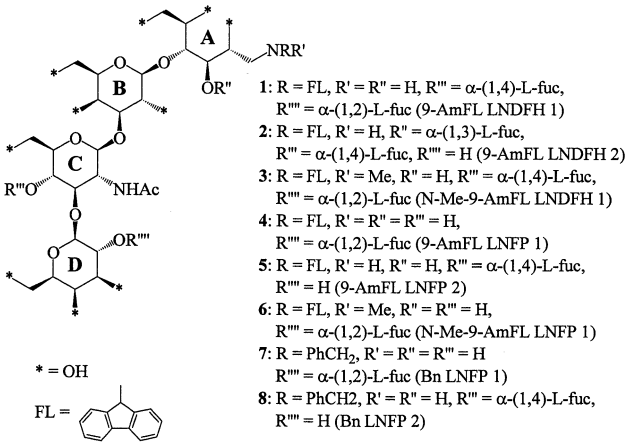

Scheme 1

fragment ion at *m/z* 714 ($C_4/Y_{4\alpha}$) lost a galactose (*m/z* 552, $C_4/Y_{3\alpha}$), a fucose (*m/z* 568, $C_4/Y_{4\alpha}/Y_{3\beta}$), and both (*m/z* 406, $C_4/Y_{3\alpha}/Y_{4\alpha}$).

The CID spectrum of the protonated species (Figure 1b, *m/z* 1165) showed a less complicated fragmentation pattern. The CID spectrum was characterized by fragments at *m/z* 1019 ($Y_{4\alpha}$ or $Y_{3\beta}$), 857 ($Y_{3\alpha}$), 508 (Y_2), 346 (Y_1), 204 (internal B/Y ion for the GlcNAc residue) and 165 (resonance-stabilized cation of the fluorene label). However, an unusual second fragmentation pathway was observed at this point. The fragment at *m/z* 654 corresponded to the loss of a single fucose ($\mathbf{D}^{\beta}$ or $\mathbf{E}^{\alpha}$ ring), a galactose ($\mathbf{D}^{\alpha}$ ring), and an N-acetyl-glucosamine (**C** ring) with retention of the second fucose unit at the remainder of the molecule. The ion at *m/z* 654 further lost a galactose (**B** ring) to give *m/z* 492 with the second fucose still attached to the ion. These fragments could be explained by invoking an unprecedented long-range transfer of a fucose unit ($\mathbf{E}^{\alpha}$ or $\mathbf{D}^{\beta}$ ring) to the open-chain terminus (**A** ring) of the oligosaccharide or to ring **B**.

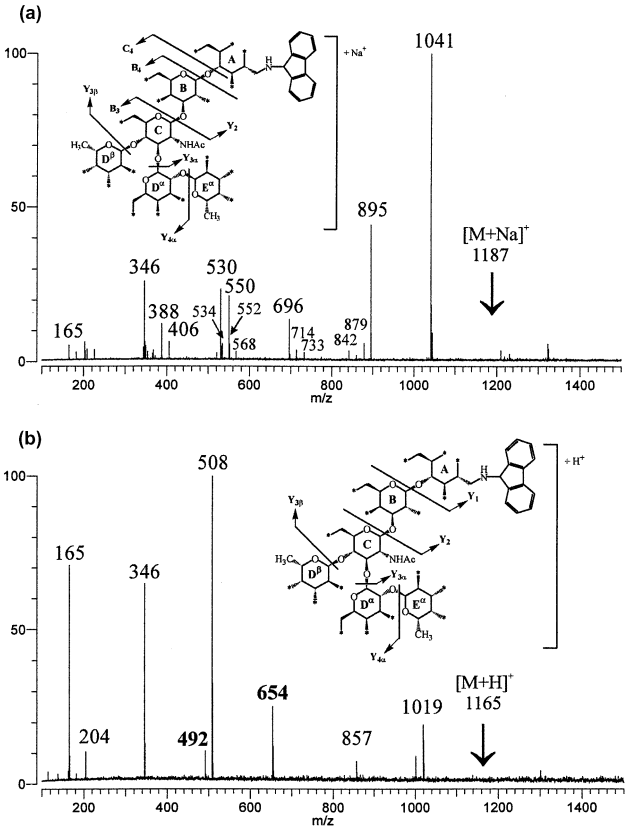

Figure 1. (**a**) FTMS-CID spectrum of Compound **1**, $[M + Na]^+$, *m/z* 1187; (**b**) CID spectrum of Compound **1**, $[M + H]^+$, *m/z* 1165. Note: The arrow indicates the position of the molecular ion prior to CID. The peak at *m/z* 1001 (not labeled) was due to electronic noise. Fragment ions at *m/z* 654 and 492 were due to long-range glycosyl transfer of a fucose.

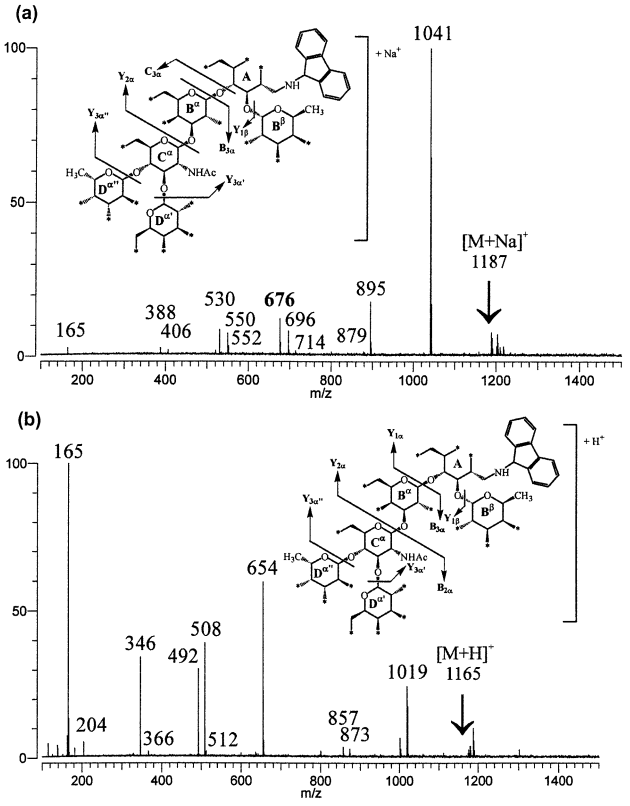

Figure 2. (**a**) FTMS-CID spectrum of Compound **2**, $[M + Na]^+$, *m/z* 1187; (**b**) CID spectrum of Compound **2**, $[M + H]^+$, *m/z* 1165. Note: The arrow indicates the position of the molecular ion prior to CID. Fragment ions at *m/z* 654 and 492 were consistent with the molecular structure.

The possibility that LNDFH I impurities were present in LNDFH II and vice versa prior to derivatization could be ruled out based on the sodiated Compound **2** (Figure 2a). The CID of the sodiated quasimolecular ion produced *m/z* 676 that corresponded to a $Y_{2\alpha}$ cleavage. Had LNDFH II been present as an impurity in LNDFH I, the same fragment would have been observed in the spectrum of $[M + Na]^+$ of Compound **1** where it is completely absent (Figure 1a). An additional argument against positional isomers as impurities could be derived from the CID spectra of the $[M + H]^+$ species. The *m/z* 654 is an abundant fragment ion in the

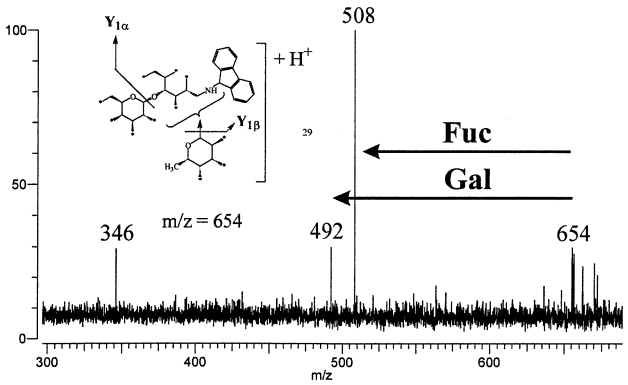

Figure 3. CID-spectrum of fragment ion at *m/z* 654 isolated from the MALDI spectrum of Compound **1** (Figure 1b, $[M + H]^+$).

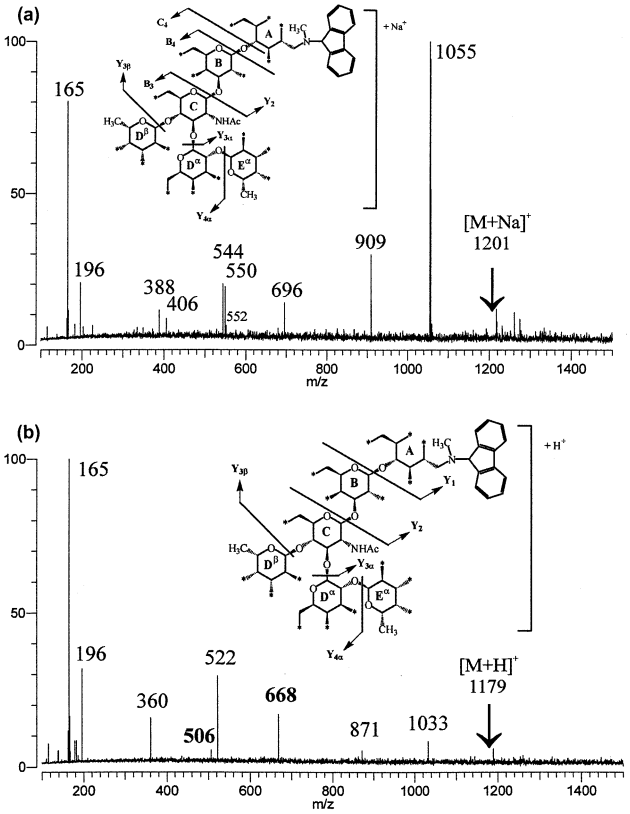

Figure 4. (**a**) FTMS-CID spectrum of Compound **3**, $[M + Na]^+$, *m/z* 1201; (**b**) CID spectrum of Compound **3**, $[M + H]^+$, *m/z* 1179.

CID spectrum of Compound **2** (Figure 2b). When compared to the corresponding signal in the CID spectrum of Compound **1** (Figure 1b), the signal intensity would suggest a large LNDFH II impurity of 20–40%. However, the CID spectrum of the $[M + Na]^+$ species (Figure 1a) indicated a relatively pure LNDFH I derivative suggesting that the native LNDFH I was free of positional isomers.

We performed a series of experiments to determine the destination of the migrating fucose in Compound **1**. A CID experiment on the isolated MALDI-generated fragment at *m/z* 654 from Compound **1** (Figure 3) clearly showed that the ion lost a fucose (*m/z* 508), a galactose (*m/z* 492), and both (*m/z* 346). The findings of the CID experiment were consistent with the proposed migration to one of the hydroxyl groups in the open chain (**A**) of Compound **1** or to the amine nitrogen at the label. The final destination of the migrating fucose will be discussed in detail further below.

To determine if the fucose was transferred to the nitrogen we N-methylated 9-AmFL-LNDFH I (Compound **1**) with methyl iodide/$NaHCO_3$ to afford Compound **3**. This would effectively diminish the transfer by introducing steric hindrance making the nitrogen less accessible. The sodium-coordinated species of Compound **3** was mass-shifted by 14 u (*m/z* 1201, Figure 4a). The CID of *m/z* 1201 produced fragments at *m/z* 1055 ($Y_{4\alpha}$ or $Y_{3\beta}$), 909 ($Y_{4\alpha}$ and $Y_{3\beta}$), and 544 (Y_2). A second series of ions corresponding to *m/z* 696 ($B_4/Y_{4\alpha}$ or $B_4/Y_{3\beta}$), 550 ($B_4/Y_{4\alpha}/Y_{3\beta}$), and 388 ($B_4/Y_{3\alpha}$) were due to the loss of the corresponding labeled residues.

The CID experiment of the protonated molecule at *m/z* 1179 (Figure 4b) yielded fragments at *m/z* 1033 ($Y_{4\alpha}$), 871 ($Y_{3\alpha}$), 522 (Y_2), 360 (Y_1), and 165 (resonance-stabilized cation of the fluorene label) that are consistent with the known structure. The fragments at *m/z* 668 and 506 were consistent with a long-range transfer reaction of a fucose (vide supra). It appeared that N-methylation did not significantly affect the relative intensities of these fragment ions suggesting that the fucose was transferred to a hydroxyl group, possibly in the open-chain, rather than the amine nitrogen.

We hoped to obtain additional information by methylation of the OH-groups. Protection of the OH-groups in Compound **1** would shut down the migration of fucose, if indeed migration to the OH-groups occurred. However, attempts at per-O-methylation of Compound **1** were futile. A deep purple coloration of the solution during treatment with NaOH in the presence of methyl iodide was observed due to the formation of an extensively resonance-stabilized carbanion at the methylene unit of the fluorene. The carbanion may have prevented the deprotonation of nearby hydroxyl groups, which is necessary for methylation.

In order to determine the fucose that had the greater propensity to undergo migration we derivatized lacto-*N*-fucopentaose I (LNFP I) and lacto-*N*-fucopentaose II (LNFP II) with 9-AmFL (Compounds **4** and **5**, respectively). The fragmentation behavior of the sodiated Compound **4** (*m/z* 1041, Figure 5a) was analogous to that of Compound **1** (Figure 1a). Fragments at *m/z* 895 (Y_4), 733 (Y_3), and 530 (Y_2) corresponded to ions with retention of the label. A second series was due to the loss of labeled residues yielding fragment ions at *m/z* 696 (B_4), and 714 (C_4). The fragment ion at *m/z* 696 lost either a fucose (*m/z* 550, B_4/Y_4), a galactose (*m/z* 534, B_3), or both (*m/z* 388, B_4/Y_3). The fragment at *m/z* 714 lost either a single fucose (*m/z* 568, C_4/Y_4), a single galactose (*m/z* 552, internal ion B_2/Y_4), or both (*m/z* 406, C_4/Y_3) in the same fashion as discussed for *m/z* 696.

The CID spectrum of the protonated Compound **4**

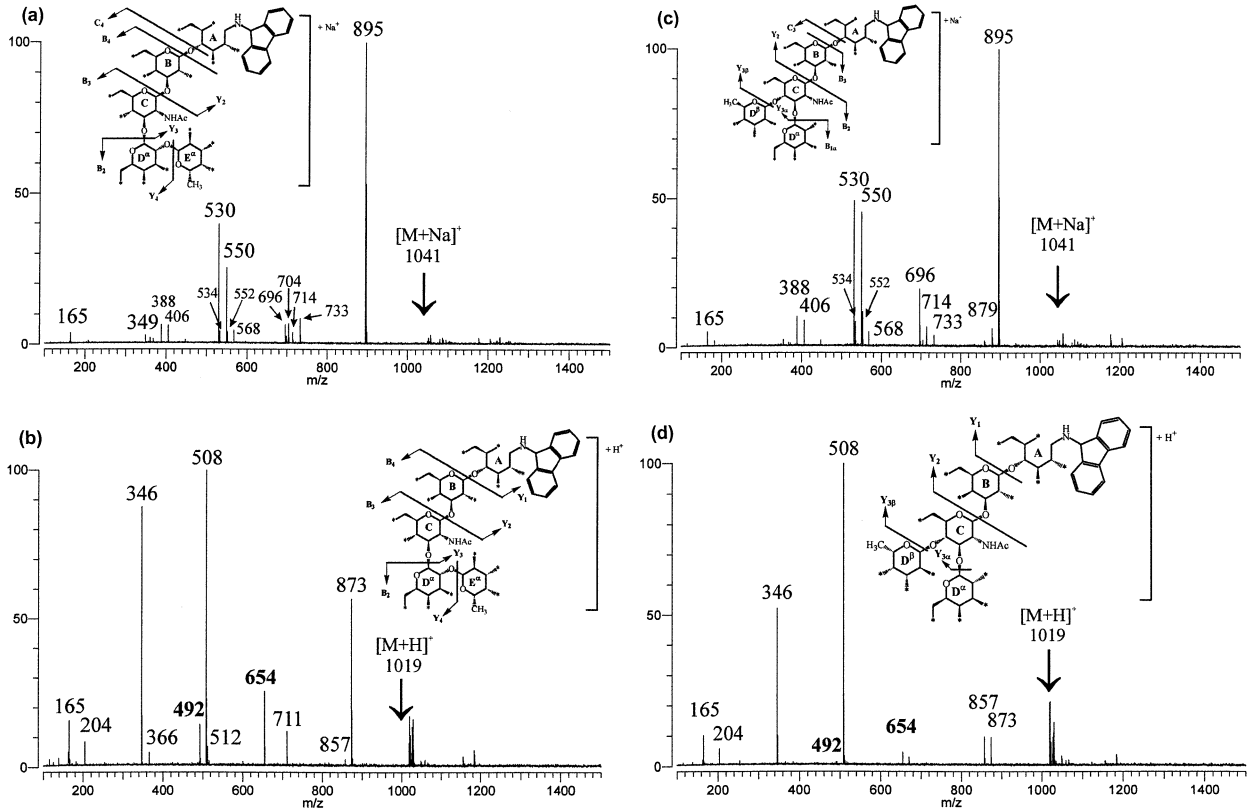

Figure 5. (**a**) FTMS-CID spectrum of Compound **4**, [M + Na]$^+$, *m/z* 1041. The signals at *m/z* 704 and 349 were due to unidentified chemical background; (**b**) CID spectrum of Compound **4**, [M + H]$^+$, *m/z* 1019; (**c**) CID spectrum of Compound **5**, [M + Na]$^+$, *m/z* 1041; (**d**) CID spectrum of Compound **5**, [M + H]$^+$, *m/z* 1019.

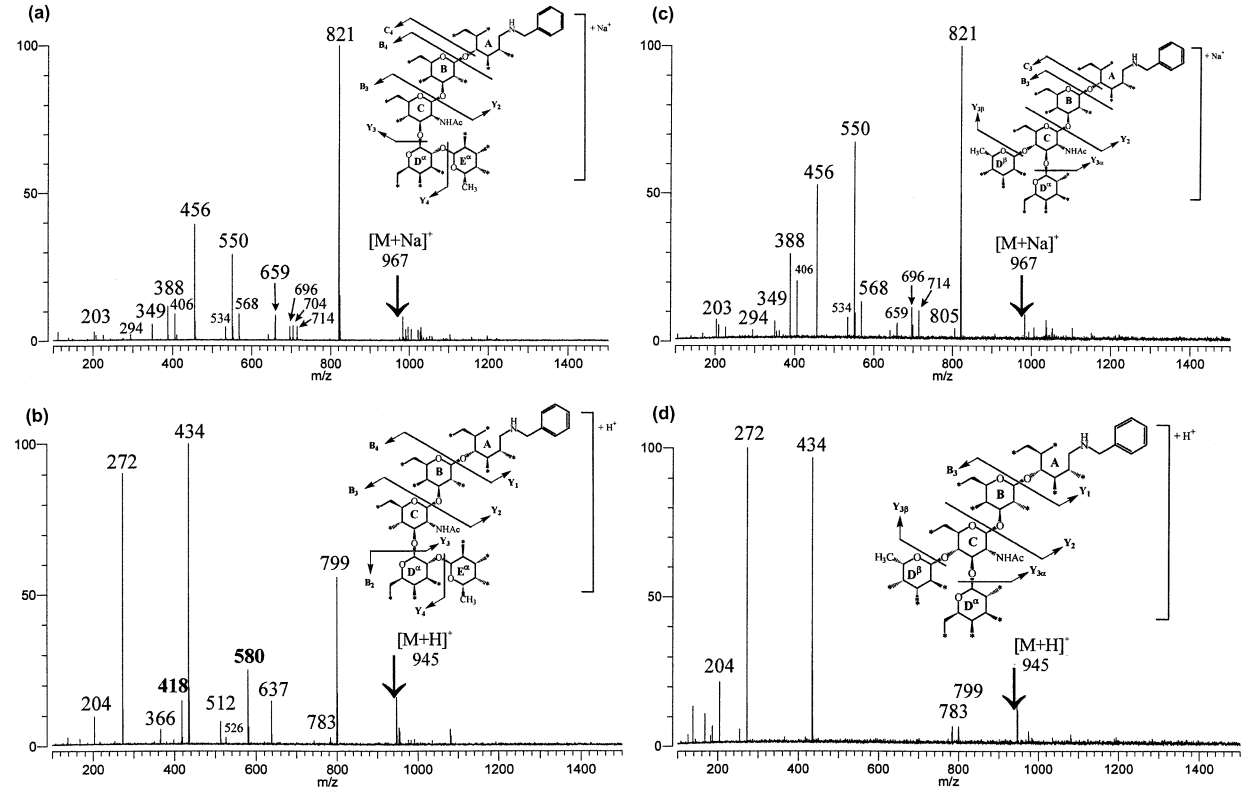

Figure 6. (**a**) FTMS-CID spectrum of Compound **7**, [M + Na]$^+$, *m/z* 967. The signals at *m/z* 704 and 349 were due to unidentified chemical background.; (**b**) CID spectrum of Compound **7**, [M + H]$^+$, *m/z* 945; (**c**) CID spectrum of Compound **8**, [M + Na]$^+$, *m/z* 967; (**d**) CID spectrum of Compound **8**, [M + H]$^+$, *m/z* 945.

Table 1. Typical fragment ions observed in CID experiments wih sodiated or protonated molecules from Compounds **1**, **3**, **4**, **6**, **7**, which have the LNFP I backbone. Given are *m/z* values of the fragments

	1		3		4		6		7	
Isol.	Na^+	H^+	Na^+	H^+	Na^+	H^+	Na^+	H^+	Na^+	H^+
Y_1	–	346.165	–	360.180	–	346.165	–	360.182	–	272.149
Y_2	530.200	508.218	544.217	522.235	530.210	508.217	544.224	522.236	456.190	434.203
Y_3	n/a	n/a	n/a	n/a	733.300	711.299	747.314	725.319	659.278	637.284
$Y_{3\alpha}$	879.342	857.357	–	871.375	n/a	n/a	n/a	n/a	n/a	n/a
$Y_{3\beta}$	1041.396	1019.415	1055.417	1033.430	n/a	n/a	n/a	n/a	n/a	n/a
Y_4	n/a	n/a	n/a	n/a	895.360	873.353	909.373	887.375	821.337	799.340
$Y_{4\alpha}$	1041.396	1019.415	1055.417	1033.430	n/a	n/a	n/a	n/a	n/a	n/a
$Y_{4\alpha}/Y_{3\beta}$	895.336	–	909.355	–	n/a	n/a	n/a	n/a	n/a	n/a
$Y_{3\alpha}/Y_{3\beta}$	733.286	–	–	–	n/a	n/a	n/a	n/a	n/a	n/a
B_3	–	–	–	–	534.190	512.198	534.187	512.199	534.189	512.200
B_3/Y_4	n/a	n/a	n/a	n/a	388.127	366.140	388.125	366	388.126	366.140
$B_3/Y_{4\alpha}/Y_{3\beta}$	388.121	–	388.122	–	n/a	n/a	n/a	n/a	n/a	n/a
B_4	842.297	–	–	–	696.251	–	696.248	–	696.249	–
B_4/Y_4	n/a	n/a	n/a	n/a	550.185	–	550.183	–	550.184	–
$B_4/Y_{4\alpha}$ or $B_4/Y_{3\beta}$ or $C_4/Z_{4\alpha}$ or $C_4/Z_{3\beta}$	696.235	–	696.238	–	n/a	n/a	n/a	n/a	n/a	n/a
$B_4/Y_{4\alpha}/Y_{3\beta}$	550.175	–	550.176	–	n/a	n/a	n/a	n/a	n/a	n/a
B_4/Y_3	n/a	n/a	n/a	n/a	388.127	366.140	388.125	366.141	388.126	366.140
$B_4/Y_{3\alpha}/Y_{3\beta}$	534.180	–	–	–	n/a	n/a	n/a	n/a	n/a	n/a
$B_4/Y_{3\alpha}/Y_{3\beta}$	388.121	–	388.122		n/a	n/a	n/a	n/a	n/a	n/a
C_4	–	–	–		714.262	–	714.258	–	714.260	–
C_4/Y_4	n/a	n/a	n/a	n/a	568.195	–	–	–	568.195	–
$C_4/Y_{4\alpha}$	714.243	–	–	–	n/a	n/a	n/a	n/a	n/a	n/a
$C_4/Y_{4\alpha}/Y_{3\beta}$	568.185	–	–	–	n/a	n/a	n/a	n/a	n/a	n/a
C_4/Y_3	n/a	n/a	n/a	n/a	406.138	–	406.136	–	406.137	–
$C_4/Y_{3\alpha}$	552.191	–	522.193	–	n/a	n/a	n/a	n/a	n/a	n/a
$C_4/Y_{3\alpha}/Y_{4\alpha}$	406.132	–	406.133	–	n/a	n/a	n/a	n/a	n/a	n/a
Int. Res. Loss	–	–	–	–	552.200	857.357	552.201	–	552.201	783.341
Rearr.	–	654.277	–	668.295	–	654.277	–	668.298	–	580.262
Rearr.	–	492.223	–	506.242	–	492.223	–	506.242	–	418.208

(*m/z* 1019) showed fragment ions at m/z 873 (Y_4), 711 (Y_3), 508 (Y_2), 346 (Y_1), and 204 (internal B/Y ion for the GlcNAc residue) (Figure 5b). The presence of fragments at *m/z* 654 (25%) and 492 (15%) was observed and was consistent with the migration of a fucose. The amplitude of the CID event was identical to that for Compound **1** (Figure 1b, vide supra).

The CID spectra of sodiated and protonated Compound **5** are shown in Figure 5c and d, respectively. For the protonated molecule (*m/z* 1019, Figure 5d), the fragments at *m/z* 654 and 492 were also observed, however, in much lower abundances (~5% and ~1%, respectively). This implied that migration of the terminal α-fucose on ring $\mathbf{D}^{\alpha}$ was favored over the other α-fucose on ring **C** and that possibly the linkage position of the fucose influenced its propensity to migrate consistent with published results [50].

We introduced a methyl group at the amine nitrogen of Compound **4** to show again that the glycosyl transfer still occurred. For $[M + Na]^+$ (*m/z* 1055, spectrum not shown), the fragment ions were readily assigned according to the known structure. For $[M + H]^+$ (*m/z* 1033, spectrum not shown), the CID spectrum contained signals at *m/z* 887 (Y_4), 725 (Y_3), 522 (Y_2), 360 (Y_1), and 165 that were consistent with the molecular structure. The fragment ions at *m/z* 668 and 506 were due to the migration of a fucose.

In order to investigate the generality of the long-range transfer with respect to the label, we derivatized LNFP I and LNFP II with benzylamine. CID spectra of benzylamine-derivatized LNFP I (**7**) and LNFP II (**8**) are shown in Figure 6. The sodiated molecule of Compound **7** (Figure 6a, *m/z* 967) gave rise to fragment ions at *m/z* 821 (Y_4), 659 (Y_3), 456 (Y_2), and 294 (Y_1) that retained the label. A second series of fragment ions arising from the loss of labeled residues was also observed as *m/z* 696 (B_4), 550 (B_4/Y_4), 534 (B_3), and 388 (B_4/Y_3). A third series analogous to the second yielded *m/z* 714 (C_4), 568 (C_4/Y_4), 552 (internal ion B_2/Y_4), and 406 (C_4/Y_3).

The CID of the protonated Compound **7** (Figure 6b, *m/z* 945) yielded fragment ions at *m/z* 799 (Y_4), 637 (Y_3), 434 (Y_2), 272 (Y_1). Fragment ions at *m/z* 512 (B_3) and 366 (B_3 and Y_4) were due to the loss of the corresponding

Table 2. Typical fragment ions observed in CID experiments with sodiated or protonated molecules from Compounds **2**, **5**, **8**, which all have the LNFP II backbone. Given are *m/z* values of the fragments

	2		5		8	
Isol.	Na^+	H^+	Na^+	H^+	Na^+	H^+
Y_1	n/a	n/a	–	346.164	–	272.149
$Y_{1\alpha}$	–	492.227	n/a	n/a	n/a	n/a
$Y_{1\alpha}/Y_{1\beta}$	–	346.167	n/a	n/a	n/a	n/a
$Y_{1\beta}$	1041.402	1019.431	n/a	n/a	n/a	n/a
Y_2	n/a	n/a	530.202	508.217	456.186	434.202
$Y_{2\alpha}$	676.263	654.284	n/a	n/a	n/a	n/a
$Y_{2\alpha}/Y_{1\beta}$	530.202	508.222	n/a	n/a	n/a	n/a
$Y_{3\alpha'}/Y_{3\alpha''}$ or $Y_{3\alpha'}/Y_{1\beta}$	879.341	857.372	n/a	n/a	n/a	n/a
$Y_{3\alpha}$	n/a	n/a	879.345	857.354	805.332	783.338
$Y_{3\alpha''}$	1041.401	1019.431	n/a	n/a	n/a	n/a
$Y_{3\alpha''}/Y_{1\beta}$	895.342	873.363	n/a	n/a	n/a	n/a
$Y_{3\beta}$	n/a	n/a	895.340	873.350	821.326	799.332
$Y_{3\beta}/Y_{3\alpha}$	n/a	n/a	733.286	–	659.271	–
$B_{2\alpha}$	–	512	n/a	n/a	n/a	n/a
$B_{2\alpha}/Y_{3\alpha''}$	–	366.141	n/a	n/a	n/a	n/a
B_3	n/a	n/a	696.237	–	696.239	–
$B_3/Y_{3\alpha}$	n/a	n/a	534.183	–	534.182	–
$B_3/Y_{3\beta}$	n/a	n/a	550.177	–	550.178	–
$B_3/Y_{3\alpha}/Y_{3\beta}$	n/a	n/a	388.123	–	388.123	–
$B_{3\alpha}$	696.238	–	n/a	n/a	n/a	n/a
$B_{3\alpha}/Y_{3\alpha'}$	–	512.203	n/a	n/a	n/a	n/a
$B_{3\alpha}/Y_{3\alpha''}$	550.176		n/a	n/a	n/a	n/a
$B_{3\alpha}/Y_{3\alpha'}/Y_{3\alpha''}$	388.122	366.141	n/a	n/a	n/a	n/a
C_3	n/a	n/a	714.247	–	714.249	–
$C_{3\alpha}$	714.248	–	n/a	n/a	n/a	n/a
$C_3/Y_{3\alpha}$	n/a	n/a	552.193	–	552.194	–
$C_3/Y_{3\beta}$	n/a	n/a	568.189	–	568.190	–
$C_3/Y_{3\alpha}/Y_{3\beta}$	n/a	n/a	406.133	–	406.133	–
$C_{3\alpha}/Y_{3\alpha'}$	552.192	–	n/a	n/a	n/a	n/a
$C_{3\alpha}/Y_{3\alpha''}$	–	–	n/a	n/a	n/a	n/a
$C_{3\alpha}/Y_{3\alpha'}/Y_{3\alpha''}$	406.132	–	n/a	n/a	n/a	n/a
Rearr.	–	800.350	–	654.276	–	–
Rearr.	–	–	–	492.224	–	–

labeled residues. The fragment ions at *m/z* 580 and 418 were consistent with the long-range transfer of a fucose. These fragments have been observed in the spectra recorded by Domon and co-workers [25] for the same compound. However, the authors did not comment on their presence. In addition, the intensities of these diagnostic fragments were not very high because the experiments were performed with time-of-flight analyzers that have significantly shorter detection periods. This implies that rearrangement ions are formed more efficiently in longer MS experiments.

The CID spectrum of $[M + Na]^+$ of derivatized LNFP II (**8**) (Figure 6c) was analogous to the one from Compound **7** (Figure 6a) with the exception that both fucose (*m/z* 821, $Y_{3\beta}$) and galactose (*m/z* 805, $Y_{3\alpha}$) were lost directly from $[M + Na]^+$. The CID spectrum of $[M + H]^+$ of Compound **8** (Figure 6d) did not indicate any long-range migration of fucose. The spectrum showed fragments at *m/z* 799 ($Y_{3\beta}$), 783 ($Y_{3\alpha}$), 434 (Y_2), and 272 (Y_1). Migration of the fucose would produce fragment ions corresponding to the loss of rings $\mathbf{D}^{\alpha}$ and **C** (*m/z* 580), which was not observed in the CID spectrum. Observed fragment ions and their *m/z* values are compiled in Tables 1 and 2.

Long-range glycosyl transfers in the gas phase have been reported before in the context of sialyl Lewis isomers and lipo-chitin oligosaccharides [50, 51]. In our study the migration of the fucose occurred in sugars with a basic amino group. The rearrangement was observed only for the protonated molecules. Sodium-coordinated species did not exhibit this behavior. Migration of the fucose on ring $\mathbf{D}^{\alpha}$ dominated over the migration of the fucose on ring **C**. N-Methylation at the label did not apparently affect the migration suggesting that the fucose did not migrate to the amine nitrogen.

Previously published data from CID experiments with oligosaccharides suggested that internal saccharide losses from the sugar structure might occur by formation of monosaccharidic epoxides [53]. If the epoxide and the charge-retaining unit do not dissociate immediately upon the CID event then the rearrangement reaction could occur. One possible reaction mechanism is shown in Scheme **2a**. Following the bond dissociation a tight ion-dipole complex is formed, in

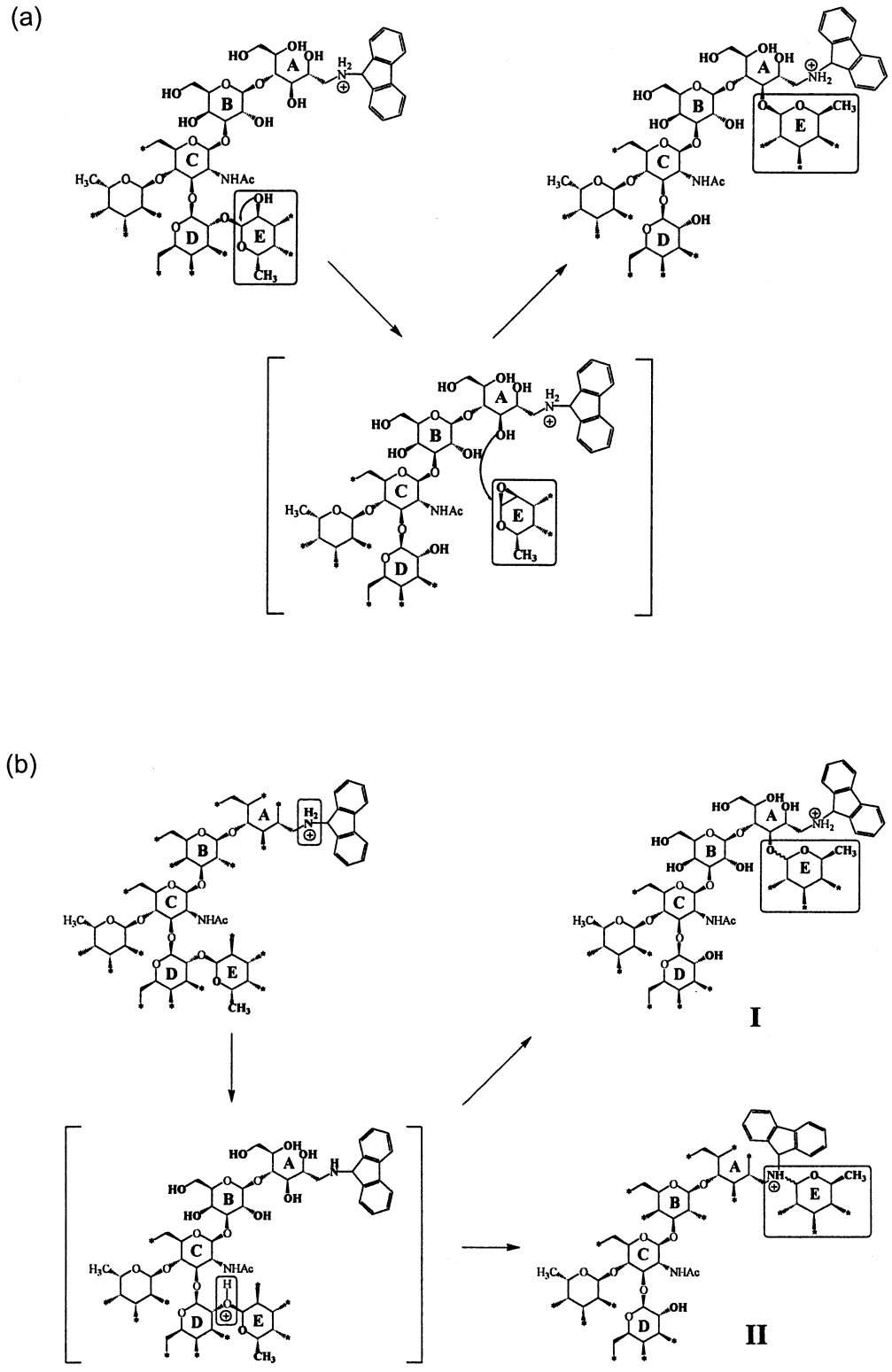

Scheme 2

which the epoxide can be opened by any of the hydroxyl groups in the open chain **A** to lead to the product. However, this rearrangement via an ion–dipole complex should not be specific for fucose. Other rearrangement reactions could involve hexoses for example (Figures 2b, 5d, and 6d) but were not observed in our case.

An alternative mechanism is outlined in Scheme **2b**. After the ionization event, the labeled Compound exists as $[M + H]^+$ in the gas-phase with the proton located at

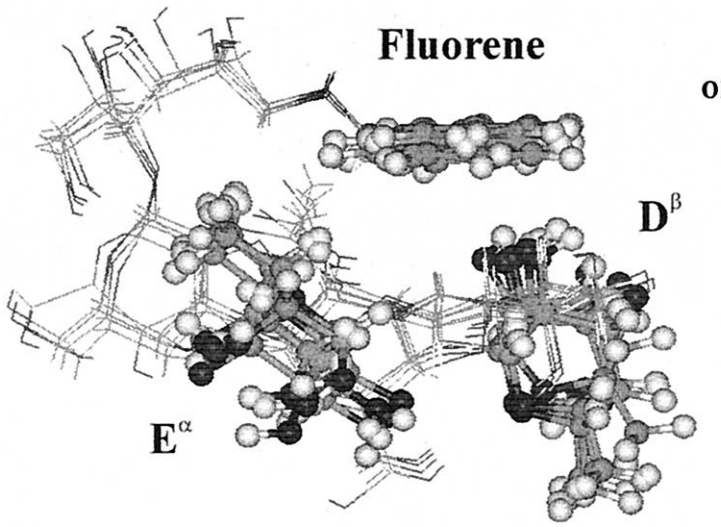

OH-group (A)	Fucose (glycosidic oxygen)	Distance (Å)
2	E^{α}	~ 7.5
3	E^{α}	~ 9.3
5	E^{α}	~ 8.9
6	E^{α}	~ 6.9
2	D^{β}	~ 11.6
3	D^{β}	~ 12.0
5	D^{β}	~ 13.5
6	D^{β}	~ 12.5

(a) Distance $N_{Fluorene}$-D^{β}: ~ 9.3 Å
Distance $N_{Fluorene}$-E^{α}: ~ 6.0 Å

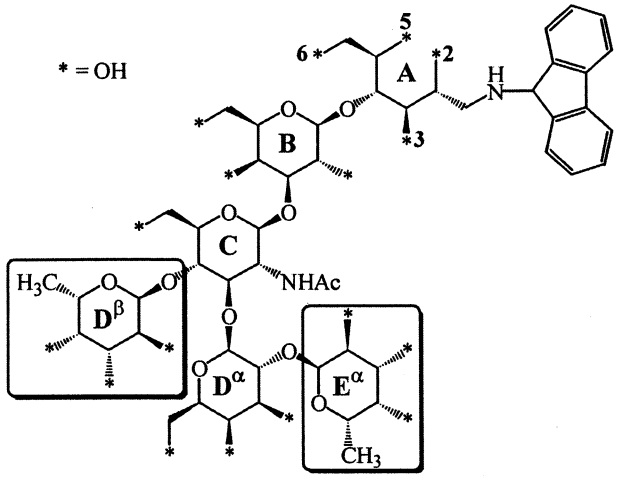

Figure 7. Molecular models of (**a**) Compound **1**; (**b**) Compound **1** protonated at amine nitrogen; (**c**) trajectory (10 ps) of the distance between the 2-hydoxyl group in ring **B** and the anomeric carbon of fucose $\mathbf{E}^{\alpha}$ at 1000 K.

the basic amine. The CID event furnishes energy to cause an intramolecular proton transfer from the ammonium unit to the glycosidic bond as shown. Subsequently, nucleophilic sites, such as the hydroxyl groups or the nitrogen can cleave the activated glycosidic bond and promote transfer to give products of Type **I** or **II**. The product of Type **II** could be ruled out based upon experimental evidence presented earlier (Figure 3).

Molecular modeling was performed to obtain information about the geometry of Compound **1** and possible reaction intermediates. Even though experimental evidence ruled out the amine nitrogen as the *destination* of migration, its role of a proton source during glycosidic bond activation was investigated. The molecular modeling results are shown in Figure 7. Low-energy structures of Compound **1** were obtained (Figure 7a) as described in the Experimental section. Structures within 3 kcal/mol of the lowest energy structure were superimposed. The fucose units and the fluorene label are highlighted as ball and stick representation. The molecules are positioned with the migrating fucose unit ($\mathbf{E}^{\alpha}$) in front of the plane. The fucose that did not migrate ($\mathbf{D}^{\beta}$) is shown behind the plane. The basic amino fluorene label is positioned as shown in the plane. The average distance between the amine nitrogen and the anomeric carbon of the migrating fucose ($\mathbf{E}^{\alpha}$) was consistently shorter (~6 Å) than the distance between the amine nitrogen and the anomeric carbon of the non-migrating fucose (~9 Å).

The protonated Compound **1** was modeled subsequently with the proton on the amine (Figure 7b). Again, structures within 3 kcal/mol of the lowest

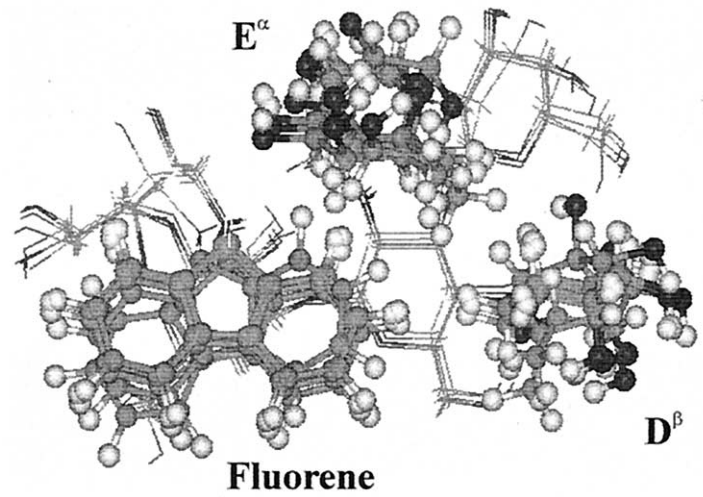

OH-group (A)	Fucose (glycosidic oxygen)	Distance (Å)
2	E^{α}	~ 7.0
3	E^{α}	~ 8.6
5	E^{α}	~ 11.1
6	E^{α}	~ 13.0
2	D^{β}	~ 10.8
3	D^{β}	~ 10.3
5	D^{β}	~ 13.7
6	D^{β}	~ 14.9

(b) Distance $N_{Fluorene}$-D^{β}: ~ 8.3 Å

Distance $N_{Fluorene}$-E^{α}: ~ 6.0 Å

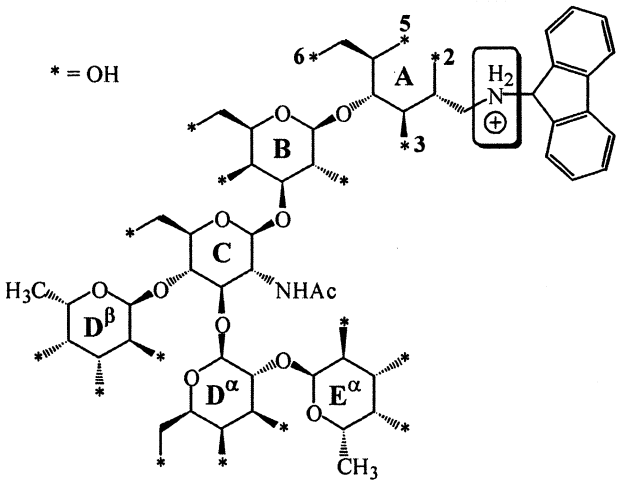

(c)

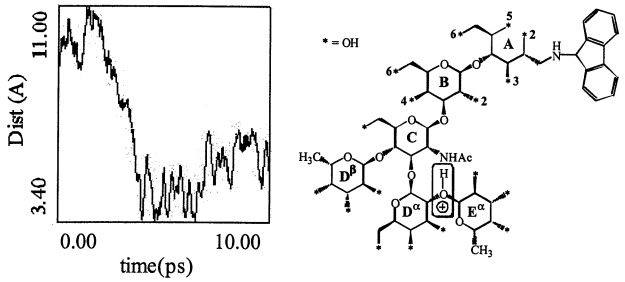

Figure 7. (Continued)

energy structure were superimposed. In Figure 7b the fluorene label and both fucose units are positioned in front of the plane. The distances between the ammonium nitrogen and the anomeric carbons of the fucose units resembled those in Figure 7a. The ammonium unit was in closer proximity (~6 Å) to the anomeric center of the migrating fucose (E^{α}). A proton transfer to the glycosidic oxygen of fucose (E^{α}) seemed reasonable as an effective activation for migration.

Compound **1** with a protonated glycosidic bond at

the migrating fucose ($\mathbf{E}^{\alpha}$) was modeled subsequently. Molecular dynamics simulation at 600 and 1000 K for 10 ps were performed starting with the lowest energy structure. The distances between the anomeric carbon of the migrating fucose $\mathbf{E}^{\alpha}$ and the OH-groups in rings **B** and **A** were measured and compared. At both temperatures, the OH-groups in ring **B** were consistently closer on average to C1-$\mathbf{E}^{\alpha}$ (~4–6 Å) than the OH-groups in the open-chain terminus **A** (~10–13 Å). The distance between C1-$\mathbf{E}^{\alpha}$ and C2-OH (ring **B**) during the simulation at 1000 K is shown in Figure 7c. The molecular modeling results showed that this distance can be as low as 3.4 Å at 1000 K. Presumably higher temperatures are obtainable during CID. However, experimental evidences pointed to the open-chain terminus (**A**) as the final destination of the fucose. This finding might imply that the intramolecular long-range transfer happened in a stepwise fashion. The first rearrangement caused the fucose to migrate to ring **B**. The second rearrangement caused the fucose to migrate to the open-chain terminus **A**. The fragment ion at *m/z* 654 possibly represented a combination of **B**- and **A**-rearranged species while *m/z* 492 resulted from a loss of galactose from only the **A**-rearranged species.

Conclusion

Several branched oligosaccharides were derivatized with benzylamine and 9-aminofluorene. In CID experiments, the sodiated species could be used to derive sequence information. The spectra were complicated by the presence of several fragmentation pathways. The spectra of the protonated species had a simplified appearance and were dominated mainly by Y-fragments. For the 9-AmFL and benzylamine derivatives of LNDFH I and LNFP I, a long-range glycosyl transfer reaction in the gas phase was observed. The transfer occurred only in the CID experiments with protonated species and is assumed to be a two-step proton-catalyzed mechanism. Both proposed mechanisms (ion-dipole and proton-catalyzed) are feasible, however, molecular modeling results supported the latter more adequately. The fucose on ring $\mathbf{D}^{\alpha}$ had a greater propensity for long-range transfer than the fucose on ring **C**. Whether this tendency was merely due to steric factors and/or the structural position of the fucoses (1,2-linkage versus 1,4-linkage) could not be investigated.

This report of an intramolecular long-range glycosyl transfer in the gas phase supports previously published results. In view of the importance that mass spectrometry plays in the analysis and structural elucidation of oligosaccharides from biological sources, we believe that long-range glycosyl transfer reactions have to be borne in mind when embarking on sequence analysis of labeled branched oligosaccharides that have a basic site.

Acknowledgments

The authors gratefully acknowledge the funding provided by the National Institute of Health.

References

1. Mori, T.; Guo, M. W.; Sato, E.; Baba, T.; Takasaki, S.; Mori, E. Molecular and Immunological Approaches to Mammalian Fertilization. *J. Reprod. Immunol.* **2000,** *47,* 139–158.
2. Sugahara, K.; Yamada, S. Structure and Function of Oversulfated Chondroitin Sulfate Variants: Unique Sulfation Patterns and Neuroregulatory Activities. *Trends Glycosci. Glycotechnol.* **2000,** *12,* 321–349.
3. Kunz, C.; Rudloff, S.; Baier, W.; Klein, N.; Strobel, S. Oligosaccharides in Human Milk: Structural, Functional, and Metabolic Aspects. *Annu. Rev. Nutr.* **2000,** *20,* 699–722.
4. Kimura, Y. Structural Features of Free N-glycans Occurring in Developing or Growing Plant Cells and Functional Feature of Plant Endo-β-N-acetylglucosaminidase. *Trends Glycosci. Glycotechnol* **2000,** *12,* 103.
5. Simanek, E. E.; McGarvey, G. J.; Jablonowski, J. A.; Wong, C.-H. Selectin–Carbohydrate Interactions: From Natural Ligands to Designed Mimics. *Chem. Rev.* **1998,** *98,* 833–862.
6. Dwek, R. A. Glycobiology: Toward Understanding the Function of Sugars. *Chem. Rev.* **1996,** *96,* 683–720.
7. Parodi, A. J. Protein Glucosylation and Its Role in Protein Folding. *Annu. Rev. Biochem.* **2000,** *69,* 69–93.
8. Prydz, K.; Dalen, K. T. Synthesis and Sorting of Proteoglycans. *J. Cell Sci.* **2000,** *113,* 193–205.
9. Coppin, A.; Maes, E.; Morelle, W.; Strecker, G. Structural Analysis of 13 Neutral Oligosaccharide-Alditols Released by Reductive beta-Elimination from Oviductal Mucins of Rana temporaria. *Eur. J. Biochem.* **1999,** *266,* 94–104.
10. Stahl, B.; Thurl, S.; Zeng, J. R.; Karas, M.; Hillenkamp, F.; Steup, M.; Sawatzi, G. Oligosacharides from Human Milk as Revealed by Matrix-Assisted Laser Desorption Ionization Mass Spectrometry. *Anal. Biochem.* **1994,** *223,* 218–226.
11. Martin, W. B.; Silly, L.; Murphy, C. M.; Raley, T. J. J.; Cotter, R. J.; Bean, M. F. Fragmentation of Carbohydrates in Laser Desorption, Plasma Desorption, and Fast Atom Bombardment Mass Spectrometry. *Int. J. Mass Spectrom. Ion Processes* **1989,** *92,* 243–265.
12. Tseng, K.; Hedrick, J. L.; Lebrilla, C. B. Catalog-Library Approach for the Rapid and Sensitive Structural Elucidation of Oligosaccharides. *Anal. Chem.* **1999,** *71,* 3747–3754.
13. Sato, Y.; Suzuki, M.; Nirasawa, T.; Suzuki, A.; Endo, T. Micro-Sequencing of Glycans Using 2-Aminobenzamide and MALDI-TOF Mass Spectrometry: Occurrence of Unique Linkage-Dependent Fragmentation. *Anal. Chem.* **2000,** *72,* 1207–1216.
14. Zaia, J.; Costello, C. E. Compositional Analysis of Glycosaminoglycans by Electrospray Mass Spectrometry. *Anal. Chem.* **2001,** *73,* 233–239.
15. Wheeler, S. F.; Harvey, D. J. Negative Ion Mass Spectrometry of Sialylated Carbohydrates: Discrimination of N-Acetylneuraminic Acid Linkages by MALDI-TOF and ESI-TOF Mass Spectrometry. *Anal. Chem.* **2000,** *72,* 5027–5039.
16. Chai, W.; Piskarev, V.; Lawson, A. M. Negative-Ion Electrospray Mass Spectrometry of Neutral Underivatized Oligosaccharides. *Anal. Chem.* **2001,** *73,* 651–657.
17. Harvey, D. J.; Bateman, R. H.; Green, M. R. High-Energy Collision-Induced Fragmentation of Complex Oligosaccharides Ionized by Matrix-Assisted Laser Desorption/Ionization Mass Spectrometry. *J. Mass Spectrom.* **1997,** *32,* 167–187.
18. Kovácik, V.; Hirsch, J.; Heerma, W. Linkage Determination of Alditol Disaccharides Using High-Energy Collision-Induced

Dissociation Spectra of Sodium Cationized Molecules. *Rapid Commun. Mass Spectrom.* **1997,** *11,* 1353–1356.
19. Orlando, R.; Bush, C. A.; Fenselau, C. Structural Analysis of Oligosaccharides by Tandem Mass Spectrometry: Collisional Activation of Sodium Adduct Ions. *Biomed. Environ. Mass Spectrom* **1990,** *19,* 747–754.
20. Küster, B.; Naven, T. J. P.; Harvey, D. J. Effect of the Reducing-Terminal Substituents on the High Energy Collision-Induced Dissociation on Matrix-Assisted Laser Desorption/Ionization Mass Spectra of Oligosaccharides. *Rapid Commun. Mass Spectrom.* **1996,** *10,* 1645–1651.
21. Charlwood, J.; Birrell, H.; Gribble, A.; Burdes, V.; Tolson, D.; Camilleri, P. A Probe for the Versatile Analysis and Characterization of N-Linked Oligosaccharides. *Anal. Chem.* **2000,** *72,* 1453–1461.
22. Mizuno, Y.; Sasagawa, T.; Dohmae, N.; Takio, K. An Automated Interpretation of MALDI/TOF Postsource Decay Spectra of Oligosaccharides. 1. Automated Peak Assignment. *Anal. Chem.* **1999,** *71,* 4764–4771.
23. Garozzo, D.; Nasello, V.; Spina, E.; Sturiale, L. Discrimination of Isomeric Oligosaccharides and Sequencing of Unknowns by Post Source Decay Matrix-Assisted Laser Desorption/Ionization Time-of-Flight Mass Spectrometry. *Rapid Commun. Mass Spectrom.* **1997,** *11,* 1561–1566.
24. Spengler, B.; Kirsch, D.; Kaufman, R.; Lemoine, J. Structure Analysis of Branched Oligosacchiardes using Post-source Decay in Matrix-Assisted Laser Desorption Ionization Mass Spectrometry. *J. Mass Spectrom.* **1995,** *30,* 782–787.
25. Lemoine, J.; Chirat, F.; Domon, B. Structural Analysis of Derivatized Oligosaccharides Using Post-Source Decay Matrix-Assisted Laser Desorption/Ionization Mass Spectrometry. *J. Mass Spectrom.* **1996,** *31,* 908–912.
26. Naven, T. J. P.; Harvey, D. J.; Brown, J.; Critchley, G. Fragmentation of Complex Carbohydrates Following Ionization by Matrix-Assisted Laser Desorption with an Instrument Fitted with Time-Lag Focusing. *Rapid Commun. Mass Spectrom.* **1997,** *11,* 1681–1686.
27. Gaucher, S. P.; Morrow, J.; Leary, J. A. STAT: A Saccharide Topology Analysis Tool Used in Combination with Tandem Mass Spectrometry. *Anal. Chem.* **2000,** *72,* 2331–2336.
28. Smith, G.; Leary, J. A. Differentiation of Stereochemistry of Glycosidic Bond Configuration: Tandem Mass Spectrometry of Diastereomeric Cobalt-Glucosyl-Glucose Disaccharide Complexes. *J. Am. Soc. Mass Spectrom.* **1996,** *7,* 953–957.
29. Li, D. T.; Her, G. R. Structural Analysis of Chromophore-Labeled Disaccharides and Oligosaccharides by Electrospray Ionization Mass Spectrometry and High-Performance Liquid Chromatography/Electrospray Ionization Mass Spectrometry. *J. Mass Spectrom.* **1998,** *33,* 644–652.
30. Mulroney, B.; Traeger, J. C.; Stone, B. A. Determination of Both Linkage Position and Anomeric Configuration in Underivatized Glucopyranosyl Disaccharides by Electrospray Mass Spectrometry. *J. Mass Spectrom.* **1995,** *30,* 1277–1283.
31. Pare, J. R. J. Stereochemical Characterization of the Glycosidic Bond by Fast-Atom-Bombardment Mass Spectrometry. *Spectroscopy* **1993,** *11,* 157–160.
32. Khoo, K. H.; Dell, A. Assignment of Anomeric Configurations of Pyranose Sugars in Oligosaccharides Using a Sensitive FAB-MS Strategy. *Glycobiol* **1990,** *1,* 83–91.
33. Domon, B.; Mueller, D. R.; Richter, W. J. Determination of Interglycosidic Linkages in Disaccharides by High Performance Tandem Mass Spectrometry. *Int. J. Mass Spectrom. Ion Processes* **1990,** *100,* 301–311.
34. Domon, B.; Mueller, D. R.; Richter, W. J. Identification of Interglycosidic Linkages and Sugar Constituents in Disaccharide Subunits of Larger Glycosides by Tandem Mass Spectrometry. *Org. Mass Spectrom.* **1989,** *24,* 357–359.
35. Cancilla, M. T.; Gaucher, S. P.; Desaire, H.; Leary, J. A. Combined Partial Acid Hydrolysis and Electrospray Ionization-Mass Spectrometry for the Structural Determination of Oligosaccharides. *Anal. Chem.* **2000,** *72,* 2901–2907.
36. Zhou, Z.; Ogden, S.; Leary, J. A. Linkage Position Determination in Oligosaccharides: MS/MS Study of Lithium-Cationized Carbohydrates. *J. Org. Chem.* **1990,** *55,* 5444–5446.
37. Hofmeister, G. E.; Zhou, Z.; Leary, J. A. Linkage Position Determination in Lithium-Cationized Disaccharides: Tandem Mass Spectrometry and Semiempirical Calculations. *J. Am. Chem. Soc.* **1991,** *113,* 5964–5970.
38. Yoon, E.; Laine, R. A. Linkage Position Determination in a Novel Set of Permethylated Neutral Trisaccharides by Collisional-Induced Dissocation and Tandem Mass Spectrometry. *Org. Mass Spectrom.* **1992**, 479–485.
39. Xie, Y.; Tseng, K.; Hedrick, J. L.; Lebrilla, C. B. Targeted Use of Exoglycosidase Digestion for the Structural Elucidation of Neutral O-linked Oligosaccharides. *J. Am. Soc. Mass Spectrom.* **2001,** *12,* 877–884.
40. Harvey, D. J.; Rudd, P. M.; Bateman, R. H.; Bordoli, R. S.; Howes, K.; Hoyes, J. B.; Vickers, R. G. Examination of Complex Oligosaccharides by Matrix-Assisted Laser Desorption/Ionization Mass Spectrometry on Time-of-Flight and Magnetic Sector Instruments. *Org. Mass Spectrom.* **1994,** *29,* 753–765.
41. Reinhold, V. N.; Reinhold, B. B.; Costello, C. E. Carbohydrate Molecular Weight Profiling, Sequence, Linkage, and Branching Data: ES-MS and CID. *Anal. Chem.* **1995,** *67,* 1772–1784.
42. Phillips, N. J.; Apicella, M. A.; Griffiss, J. M.; Gibson, B. W. Structural Studies of the Lipooligosaccharides from Haemophilus influenzae Type b Strain A2. *Biochemistry* **1993,** *32,* 2003–2012.
43. Burlingame, A. L.; Boyd, R. K.; Gaskell, S. J. Mass Spectrometry. *Anal. Chem.* **1994,** *66,* 634R–683R.
44. Yang, Y.; Orlando, R. Simplifying the Exoglycosidase Digestion/MALDI-MS Procedures for Sequencing N-Linked Carbohydrate Side Chains. *Anal. Chem.* **1996,** *68,* 570–572.
45. Mechref, Y.; Novotny, M. V. Mass Spectrometric Mapping and Sequencing of N-Linked Oligosaccharides Derived from Submicrogram Amounts of Glycoproteins. *Anal. Chem.* **1998,** *70,* 455–463.
46. Colangelo, J.; Orlando, R. On-Target Exoglycosidase Digestions/MALDI-MS for Determining the Primary Structures of Carbohydrate Chains. *Anal. Chem.* **1999,** *71,* 1479–1482.
47. Geyer, H.; Schmitt, S.; Wuhrer, M.; Geyer, R. Structural Analysis of Glycoconjugates by On-Target Enzymic Digestion and MALDI-TOF-MS. *Anal. Chem.* **1999,** *71,* 476–482.
48. Franz, A. H.; Molinski, T. F.; Lebrilla, C. B. MALDI-FTMS Characterization of Oligosaccharides Labeled with 9-Aminofluorene. *J. Am. Soc. Mass Spectrom.* **2001,** *12,* 1254–1261.
49. Broberg, S.; Broberg, A.; Duus, J. O. Matrix-Assisted Laser Desorption/Ionization Time-of-Flight Mass Spectrometry of Oligosaccharides Derivatized by Reductive Amination and N,N-Dimethylation. *Rapid Commun. Mass Spectrom.* **2000,** *14,* 1801–1805.
50. Ernst, B.; Mueller, D. R.; Richter, W. J. False Sugar Sequence Ions in Electrospray Tandem Mass Spectrometry of Underivatized Sialyl-Lewis-type Oligosaccharides. *Int. J. Mass Spectrom. Ion Processes*, 1997;160:283–290.
51. Olsthoorn, M. M. A.; Lopez-Lara, I. M.; Petersen, B. O.; Bock, K.; Haverkamp, J.; Spaink, H. P.; Thomas-Oates, J. E. Novel Branched Nod Factor Structure Results from α-(1→3) Fucosyl Transferase Activity: The Major Lipo-Chitin Oligosaccharides from *Mesorhizobium loti* Strain NZP2213 Bear an α-(1→3) Fucosyl Substituent on a Nonterminal Backbone Residue. *Biochemistry* **1998,** *37,* 9024–9032.
52. Brull, L. P.; Heerma, W.; Thomas-Oates, J.; Haverkamp, J.; Kovacik, V.; Kovac, P. Loss of Internal 1→6 Substituted

Monosaccharide Residues from Underivatized and Per-O-Methylated Trisaccharides. *J. Am. Soc. Mass Spectrom.* **1997,** *8,* 43–49.
53. Kovacik, V.; Hirsch, J.; Kovac, P.; Heerma, W.; Thomas-Oates, J.; Haverkamp, J. Oligosaccharide Characterization Using Collision-Induced Dissociation Fast Atom Bombardment Mass Spectrometry: Evidence for Internal Monosaccharide Residue Loss. *J. Mass Spectrom.* **1995,** *30,* 949–958.
54. McNeil, M. Elimination of Internal Glycosyl Residues During Chemical Ionization-Mass Spectrometry of Per-O-Alkylated Oligosaccharide-Alditols. *Carbohydr. Res.* **1983,** *123,* 31–40.
55. Thorne, G. C.; Ballard, K. D.; Gaskell, S. J. Metastable Decomposition of Peptide [M + H]+ Ions Via Rearrangement Involving Loss of C-Terminal Amino Acid Residue. *J. Am. Soc. Mass Spectrom.* **1990,** *1,* 249–257.
56. Cancilla, M. T.; Wong, A. W.; Voss, L. R.; Lebrilla, C. B. Fragmentation Reactions in the Mass Spectrometry Analysis of Neutral Oligosaccharides. *Anal. Chem.* **1999,** *71,* 3206–3218.
57. Cancilla, M. T.; Penn, S. G.; Lebrilla, C. B. Alkaline Degradation of Oligosaccharides Coupled with Matrix-Assisted Laser Desorption/Ionization Fourier Transform Mass Spectrometry: A Method for Sequencing Oligosaccharides. *Anal. Chem.* **1998,** *70,* 663–672.
58. Tseng, K.; Lindsay, L. L.; Penn, S.; Hedrick, J. L.; Lebrilla, C. B. Characterization of Neutral Oligosaccharide-Alditols from Xenopus laevis Egg Jelly Coats by Matrix-Assisted Laser Desorption Fourier Transform Mass Spectrometry. *Anal. Biochem.* **1997,** *250,* 18–28.
59. Packer, N. H.; Lawson, M. A.; Jardine, D. R.; Redmond, J. W. A General Approach to Desalting Oligosaccharides Released from Glycoproteins. *Glycoconj. J.* **1998,** *15,* 737–747.
60. Ramirez, J.; Ahn, S.; Grigorean, G.; Lebrilla, C. B. Evidence for the Formation of Gas-Phase Inclusion Complexes with Cyclodextrins and Amino Acids. *J. Am. Chem. Soc.* **2000,** *122,* 6884–6890.
61. Domon, B.; Costello, C. E. A Systematic Nomenclature for Carbohydrate Fragmentations in FAB-MS/MS Spectra of Glycoconjugates. *Glycoconj. J.* **1988,** *5,* 397–409.